Geomagnetic Conjugate Observations of Ionospheric Disturbances in response to North Korea Underground Nuclear Explosion on 3 September 2017

Yi Liu, Chen Zhou*, Qiong Tang, Guanyi Chen, and Zhengyu Zhao

Department of Space Physics, School of Electronic Information, Wuhan University, Wuhan, China

Corresponding to: chenzhou@whu.edu.cn

Key points:

1. Geomagnetic conjugate ionospheric disturbances related to UNE were observed by IGS stations and Swarm satellite.
2. Radial propagation velocity from the UNE epicenter was calculated from temporal and spatial distribution of conjugate ionospheric disturbances.
3. The ionospheric disturbances present the evidence of the LAIC electric field penetration process.

Abstract

We report observations of ionospheric disturbances in response to North Korea underground nuclear explosion (UNE) on 3 September 2017. By using data from IGS (International GNSS Service) stations and Swarm satellite, geomagnetic conjugate ionospheric disturbances were observed. The observational evidences showed that UNE-generated ionospheric disturbances propagated radially from the UNE epicenter with the velocity of ~ 280 m/s. We propose that the ionospheric disturbances are results of electrodynamic process caused by LAIC (Lithosphere-Atmosphere-Ionosphere Coupling) electric field penetration. LAIC electric field can also be mapped to the conjugate hemispheres along the magnetic field line and consequently cause ionospheric disturbances in conjugate regions. The UNE-generated LAIC electric field penetration plays an important role in the ionospheric disturbances in the region of the nuclear test site nearby and the corresponding geomagnetic conjugate points.

Key words: geomagnetic conjugate ionospheric disturbances; electrodynamic process; LAIC electric field penetration

1 Introduction

Ionospheric disturbances can be generated by various natural processes such as geomagnetic storms, internal electrodynamic instabilities and so forth. Furthermore, human activity can also cause evident ionospheric disturbances. Although underground nuclear explosion (UNE) is detonated deep in the lithosphere, ionospheric disturbances related to UNE can also be observed. By using GNSS-TEC observations, *Park et al.* (2011) reported that traveling ionospheric disturbances (TIDs) with phase velocity of ~273 m/s were generated by UNE in the 25 May 2009 North Korea UNE test. They proposed that acoustic gravity waves (AGWs) generated by the UNE can propagate to ionosphere and cause wavelike disturbances.

While the observations of UNE related ionospheric disturbances have been discussed in (*Park et al.*, 2011; 2013), further investigation is still required to understand the mechanism(s) of ionospheric disturbance generation. Lithosphere-atmosphere-ionosphere coupling (LAIC) mechanisms originally proposed to interpret the linkage between ionospheric disturbances and earthquake activities are the most likely explanation for the ionospheric disturbances in response to UNE. The AGWs theory is one part of LAIC mechanisms (*Liu et al.*, 2016; *Maruyama et al.*, 2016). AGWs excited by the unusual events in lithosphere such as an earthquake or an UNE can propagate to ionospheric height and generate TID and electromagnetic disturbances (*Gokhberg et al.*, 1990; *Pokhotelov et al.*, 1994, 1995, 1999; *Mikhailov et al.*, 2000; *Huang et al.*, 2011). However, the AGWs mechanism cannot fully explain all the observations related

to earthquakes. The electrostatic coupling is another candidate for LAIC mechanisms. During earthquakes, LAIC electric filed or current can be excited by complex physical and chemical reactions induced by rock rupture and penetrate the ionosphere to promote plasma disturbances by $\boldsymbol{E}\times\boldsymbol{B}$ motion (*Xu et al.*, 2011; *Zhao & Hao*, 2015). *Zhou et al.* (2017) developed an electric field penetration model for LAIC and their simulation results showed that the penetration height of LAIC electric field can reach to 400 km in mid-latitude regions. Because of high electric conductivity along the geomagnetic field lines, LAIC electric field can also be mapped along geomagnetic field lines and cause ionospheric disturbances at the geomagnetic conjugate points (*Ruzhin et al.*, 1998; *Zhang et al., 2009*; *Li & Parrot*, 2017).

In this study, we have used magnetic conjugate GNSS observations and Swarm satellite to investigate the LAIC electric penetration effects of North Korea UNE on 3 September 2017.

2 Instrument and Data

The IGS stations used in this study are located in East Asia and Australia. The geographical positions of the UNE and the IGS stations are showed in Figure 1. In order to eliminate the noise and multipath effects of GPS signals, only carrier phase observations are utilized to derive the relative slant total electron content (STEC). The time resolution is about 30 s. The ionospheric pierce points (IPPs) height in this study is assumed at 350 km. Figure 2 shows an example of time series of relative STEC

obtained by SUWN using satellite PRN 28 between 03:00-05:00 UT on 3 September 2017. To calculate the ionospheric disturbances related to UNE from GNSS observations, the main trends of relative STEC strongly influenced by the Sun's diurnal cycle need to be removed. In this study, the numerical third-order horizontal 3-point derivatives of relative STEC are used for extracting the ionospheric disturbances (*Park et al.*, 2011). In the first step, the numerical first-order horizontal 3-point derivatives are taken as follows:

$$\delta s_i = s_i - \frac{\left(s_{i-1} + s_{i+1}\right)}{2} \qquad i=\{2,...,n-1\} \tag{1}$$

where s_i is the i^{th} data point, δs_i is the first derivative, and n is the number of relative STEC observations. The main relative STEC trends are removed through this process. Figure 3(a) shows the time series of first-order derivatives of relative STEC. Waves with small amplitudes occurred at around 3.9 and 4.1 hours, even though it was not certain whether they were meaningful signals or just noises. The numerical derivative formula is repeatedly performed on relative STEC derivatives to extract the ionospheric disturbances related to UNE. The second-order derivatives can be written in the following expression:

$$\delta\delta s_i = \delta s_i - \frac{\left(\delta s_{i-1} + \delta s_{i+1}\right)}{2} \qquad i=\{2,...,m-1\} \tag{2}$$

where $\delta\delta s_i$ is the second derivative, and m is the number of first derivative observations. Figure 3(b) shows the time series of second-order derivatives of relative STEC. Compared to the first-order derivatives presented in Figure 3(a), the amplitude around the 3.9 hour was amplified while others were not significant. The third-order

derivatives are given as follows:

$$\delta\delta\delta s_i = \delta\delta s_i - \frac{\left(\delta\delta s_{i-1} + \delta\delta s_{i+1}\right)}{2} \quad i=\{2,...,l\text{-}1\} \tag{3}$$

where $\delta\delta\delta s_i$ is the third derivative, and l is the number of second derivative observations. Figure 3(c) shows the time series of third-order derivatives of relative STEC. Compared to the second-order derivatives presented in Figure 3(b), the disturbances around the 3.9 hour was further amplified. Therefore, compared to the standard first derivatives, the numerical third-order horizontal –point derivatives can emphasized the more significant wave components with small amplitudes. Moreover, to further remove the background noises of third-order derivatives of relative STEC, the harr wavelet decomposition process is applied to the third-order derivatives. Equations (4) and (5) give the harr wavelet function and scale function, respectively.

$$\psi_H(t) = \begin{cases} 1 & 0 \le t \le 1/2 \\ -1 & 1/2 \le t < 1 \\ 0 & \text{others} \end{cases} \tag{4}$$

$$\phi_H(t) = \begin{cases} 1 & 0 \le t < 1 \\ 0 & others \end{cases} \tag{5}$$

Figure 3(d) shows the wavelet de-noised third-order derivatives. From Figure 3(d), it was found that the background noises in Figure 3(c) were completely removed and only valuable wave components were retained.

Swarm mission operated by the European Space Agency (ESA) mainly focuses on the survey of global geomagnetic field and its temporal evolution. Swarm mission consists of three satellites named Alpha (A), Bravo (B), and Charlie (C). By using the magnetic

field data detected by Vector Field Magnetometer (VFM) on Swarm, the ionospheric radial current (IRC) density could be calculated by using spatial gradient of residual magnetic field data through Ampère's law (*Ritter et al.*, 2013). The field-aligned current (FAC) density could be also obtained by the ratio of the IRC density to the sine of the magnetic inclination angle. The FAC density and IRC density used in the study were provided by Swarm level 2 dataset with a time resolution of 1 s. The ionospheric current disturbances associated with UNE can also be calculated by the above method.

3 Observations

According to the measurements of China Earthquake Network Center (CENC), the approximate location of UNE on 3 September, 2017 is at 41.35 °N and 129.11 °E. The explosive time was at 03:30:01 UTC. The geomagnetic *K*p index was less than 3 and AE index was less than 500 nT before and after the UNE, which indicates that the geomagnetic activity was not so active.

Figure 4 shows the time sequences of 3rd-order derivatives of carrier phase derived relative STEC by GNSS observations from different IGS stations in East Asia and Australia on 3 September 2017. All the GNSS observations from northern and southern hemisphere showed obvious short-period fluctuations within 2 hours after the UNE. It was also found that time delay after the UNE was different according to different IPPs of GPS signals. Figure 5 presents the IPPs tracks of relative STEC derivatives. In order to investigate the propagation velocity of ionospheric disturbances, we assumed that

the UNE-generated ionospheric disturbances propagate radially with a certain velocity.

Figure 6 illustrates the satellite Swarm B ionospheric current derivatives. Compared to observed results of ionospheric current in quiet time, it was seen that the FAC derivatives and IRC derivatives at conjugate hemispheres both showed obvious short-period fluctuations after the UNE. The ionospheric current disturbances could reach 0.5 $\mu A \cdot m^{-2} \cdot s^{-3}$.

Based on the UNE-IPPs horizontal distances and the ionospheric disturbances arrival time, the horizontal propagation velocity of ionospheric disturbances could be estimated by linear fitting model. The horizontal distance from IPPs to epicenter and time delay of the UNE-generated ionospheric disturbances (STEC disturbances and ionospheric current disturbances) are presented in Figure 7. Black triangle and green triangle presented in Figure 7 represent the position of ionospheric current disturbances in the northern hemisphere and the geomagnetic conjugate position of ionospheric current disturbances in the southern hemisphere, respectively. The value of horizontal velocity obtained by the least square estimation was ~280 m/s.

4 Discussion

By utilizing geomagnetic conjugate GNSS TEC observations and ionospheric current products from Swarm, we introduced the ionospheric disturbances which are considered as a result of the UNE carried out by North Korea on 3 September 2017.

The method of the numerical third-order horizontal 3-point derivatives was applied to the GNSS TEC and the ionospheric current of Swarm to extract the ionospheric disturbances, which can also be found in *Park et al.*, (2011). Ionospheric disturbances derived from GNSS TEC observations in our study are consistent with the results of North Korea UNE on 25 May 2009 obtained by *Park et al.* (2011).

The effects of UNE on the ionosphere could be very similar to that of earthquakes on the ionosphere. In previous studies, AGWs are considered as the most likely mechanism for atmospheric and ionospheric disturbances excited by UNE or earthquakes (*Mikhailov et al.*, 2000; *Che et al.*, 2009; *Garrison et al.*, 2010; *Park et al.*, 2011, 2013; *Yang et al.*, 2012; *Maruyama et al.*, 2016). *Klimenko et al.* (2011) proposed that the ionospheric disturbances were generated by small-scale internal gravity waves (IGWs) through propagation and dissipation processes during seismic activity. *Liu et al.* (2016), and *Chum et al.* (2016, 2018) suggested that co-seismic ionospheric disturbances could be generated by long-period infrasound waves excited by seismic waves. However, AGWs mechanism cannot explain the geomagnetic conjugate observations in Figure 4, because mechanical waves such as AGWs cannot propagate to the other hemisphere.

Recent researches have shown that earthquake ionospheric disturbances could be attributed to not only the AGW mechanism but also the electrostatic coupling, which means the electric field or current penetration into ionosphere induced by earthquakes. Based on the observations of INTERCOSMOS-BULGARIA-1300 satellite and

185 DEMETER satellite, *Gousheva et al.* (2008, 2009) and *Zhang et al.* (2014) reported
186 ionospheric quasi-static electric field perturbations during seismic activities. By using
187 the magnetometer observations, *Hao et al.* (2013), and *Liu et al.* (2016) showed obvious
188 ionospheric current and magnetic field perturbations after the Tohoku earthquake. They
189 proposed that the seismo-traveling atmospheric disturbances (STADs) caused by
190 infrasonic waves can propagate vertically into the ionosphere and modify the *E* layer
191 Hall and Pedersen conductivity, resulting in background ionospheric electric field and
192 magnetic field disturbances. *Pulinets et al.* (2000) proposed a quasi-electrostatic model
193 for the LAIC mechanism. The simulation results indicated that the abnormal electric
194 field induced by an earthquake can penetrate into the ionosphere to cause the
195 ionospheric electric field disturbances (*Sorokin et al.*, 2001). The enhancement of TEC
196 at the epicenter and its geomagnetic conjugate points were reported by *Liu et al.* (2011),
197 which indicated that the earthquake-generated electric field penetration can be mapped
198 along geomagnetic field lines to promote ionospheric disturbances at its conjugate
199 points by electrodynamic process through $\boldsymbol{E}\times\boldsymbol{B}$ drift. Therefore, the geomagnetic
200 conjugation effects of ionospheric disturbances in Figure 4 can be explained by the
201 UNE-generated electric field penetration. A schematic sketch of geomagnetic conjugate
202 effect related to UNE in the region of the nuclear test site nearby and the corresponding
203 geomagnetic conjugate region is shown in Figure 8. The UNE-generated electric field
204 or current penetrates into the ionosphere and further generates an abnormal electric field
205 at ionospheric altitude. The distribution of ionospheric electric filed showed in Figure
206 8 were calculated by LAIC electric field penetration model proposed by *Zhou et al.*

(2017). Because of the existence of high conductivity of geomagnetic field, the abnormal ionospheric electric filed could be mapped along geomagnetic field lines. Geomagnetic conjugate ionospheric disturbances could be generated by abnormal ionospheric electric filed through $\boldsymbol{E}\times\boldsymbol{B}$ drift. Our study provides observational evidences of LAIC electric penetration other than acoustic gravity wave mechanism.

Geomagnetic conjugate observations in ionosphere have been reported by a few researchers. *Otsuka et al.* (2002; 2004) reported simultaneous observations of equatorial airglow depletions and medium-scale TIDs at geomagnetic conjugate points in both hemispheres by two all-sky imagers. Their results also suggested that polarization electric field, which is important for airglow depletion and MSTIDs generation, can be mapped along the field lines.

In our observations, we found that the ionospheric disturbances in both hemispheres caused by the UNE-generated electric field penetration propagated radially at the velocity of roughly 280 m/s in Figure 5 and Figure 7. LAIC electric field can be roughly estimated to be 14.5 mV/m, which is consistent with the magnitude of the earthquake-generated ionospheric electric field presented by *Zhang et al.* (2014). Figure 6 presents the results of the ionospheric current disturbances detected by the satellite Swarm B after the UNE. The reason may be that the ionospheric disturbances from the UNE propagate here to generate the current disturbances by electrodynamic process.

Moreover, compared with the magnitude and time scale of ionospheric disturbances caused by earthquakes, there are inconsistencies in our study. Based on IGS station observations around Tibet and Nepal, *Kong et al.* (2018) reported that TEC disturbances exceeded 0.3 TECU and lasted for 15-20 minutes during 2015 Nepal earthquake. However, it was found that the UNE-generated ionospheric disturbances were relatively smaller and lasted within 5 minutes in Figure 4. Therefore, it is possible to distinguish natural earthquakes and UNE events based on GNSS observations.

5 Summary

In this study, we have shown that the geomagnetic conjugate observations of GNSS TEC and ionospheric current from Swarm considered as a response to North Korea UNE on 3 September 2017. The LAIC electric penetration effects of UNE have been discussed in details. The main results are summarized as follows:

1. The ionospheric TEC and current disturbances were observed in both hemispheres after the UNE. According to the spatial-temporal relation, UNE-generated ionospheric disturbances propagated radially from the explosion epicenter with the velocity of ~ 280 m/s.

2. The ionospheric disturbances may be caused by LAIC electric penetration rather than AGWs. LAIC electric field induced by UNE penetrates into the ionosphere and causes plasma density disturbances near the nuclear test cite and its conjugate points by

electrodynamic process.

Acknowledgments

We thank the use of GPS-TEC data from IGS Data Center of Wuhan University (http://www.igs.gnsswhu.cn/index.php/Home/DataProduct/igs.html). We also acknowledge the ESA for the Swarm data (https://earth.esa.int/web/guest/swarm/data-access). The work is supported by the National Natural Science Foundation of China (NSFC grant No. 41574146 and 41774162).

References

Che, I.-Y., Kim, T. S., Jeon, J.-S., and Lee, H.-I.: Infrasound observation of the apparent North Korean nuclear test of 25 May 2009, Geophys. Res. Lett., 36, L22802, 2009.

Chum, J., Cabrera, M. A., Mošna, Z., Fagre, M., Baše, J., and Fišer, J.: Nonlinear acoustic waves in the viscous thermosphere and ionosphere above earthquake, J. Geophys. Res. Space Physics, 121, 2016.

Chum, J., Liu, J.-Y., Podolská, K., and Šindelářová, T.: Infrasound in the ionosphere from earthquakes and typhoons, J. Atmos. Sol. Terr. Phys., 171, 72-82, 2018.

Garrison, J. L., Yang, Y.-M., and Lee, S.-C.: Observations of ionospheric disturbances coincident with North Korean underground nuclear tests, Abstract SA43B-1754 presented at 2010 Fall Meeting, AGU, San Francisco, Calif., 13–17 Dec, 2010.

Gokhberg, M. B., Pilipenlco, V. A., Pokhotelov, O. A., and Partasaraty, S.: Acoustic disturbance induced by underground nuclear explosion as source of electrostatic turbulence in the magnetosphere, Doklady AN SSSR, 313(N3), P568-574, 1990.

Gousheva, M., Danov, D., Hristov, P., and Matova, M.: Quasi-static electric fields phenomena in the ionosphere associated with pre- and post-earthquake effects, Nat. Hazards Earth Syst. Sci., 8, 101-107, 2008.

Gousheva, M., Danov, D., Hristov, P., and Matova, M.: Ionospheric quasi-static electric field anomalies during seismic activity in August–September 1981, Nat. Hazards Earth Syst. Sci., 9, 3-15, 2009.

Huang, Q.: Retrospective investigation of geophysical data possibly associated with the Ms8.0 Wenchuan earthquake in Sichuan, China, J. Asian Earth Sci., 41(4-5): 421-

427, 2011.

Klimenko, M. V., Klimenko, V. V., Karpov, I. V., and Zakharenkova, I. E.: Simulation of Seismo-Ionospheric Effects Initiated by Internal Gravity Waves, Russ. J. Phys. Chem. B, 5(3), 393-401, 2011.

Kong, J., Yao, Y., Zhou, C., Liu, Y., Zhai, C., Wang, Z., and Liu, L.: Tridimensional reconstruction of the Co-Seismic Ionospheric Disturbance around the time of 2015 Nepal earthquake, J. Geodesy, 3, 1-12, 2018.

Li, M., and Parrot, M.: Statistical analysis of the ionospheric ion density recorded by DEMETER in the epicenter areas of earthquakes as well as in their magnetically conjugate point area, Adv. Space Res., 61(3), 974-984, 2017.

Liu, J. Y., Le, H., Chen, Y. I., Chen, C. H., Liu, L., Wan, W., Su, Y. Z., Sun, Y. Y., Lin, C. H., and Chen, M. Q.: Observations and simulations of seismo-ionospheric GPS total electron content anomalies before the 12 January 2010 M7 Haiti earthquake, J. Geophys. Res., 116, A04302, 2011.

Liu, J. Y., Chen, C. H., Sun, Y. Y., Chen, C. H., Tsai, H. F., Yen, H. Y., Chum, J., Lastovicka, J., Yang, Q. S., Chen, W. S., and Wen, S.: The vertical propagation of disturbances triggered by seismic waves of the 11 March 2011 M9.0 Tohoku earthquake over Taiwan, Geophys. Res. Lett., 43(4), 1759-1765, 2016.

Maruyama, T., Yusupov, K., and Akchurin, A.: Ionosonde tracking of infrasound wavefronts in the thermosphere launched by seismic waves after the 2010 M8.8 Chile earthquake, J. Geophys. Res. Space Physics., 121, 2683-2692, 2016.

Mikhailov, Y. M., Mikhailova, G. A., and Kapustina, O. V.: VLF effects in the outer

303 ionosphere from the underground nuclear explosion on Novaya Zemlya island on
304 24 October, 1990 (INTERCOSMOS 24 satellite data), Phys. Chem. Earth Part C,
305 25(1–2), 93–96, 2000.
306 Otsuka, Y., Shiokawa, K., Ogawa, T., and Wilkinson, P.: Geomagnetic conjugate
307 observations of equatorial airglow depletions, Geophys. Res. Lett., *29*, 1753, 2002.
308 Otsuka, Y., Shiokawa, K., Ogawa, T., and Wilkinson, P.: Geomagnetic conjugate
309 observations of medium-scale traveling ionospheric disturbances at midlatitude
310 using all-sky airglow imagers, Geophys. Res. Lett., 31, L15803, 2004.
311 Park, J., Frese, R. R. B. von, Grejner-Brzezinska, D. A., Morton, Y., and Gaya-Pique,
312 L. R.: Ionospheric detection of the 25 May 2009 North Korean underground
313 nuclear test, Geophys. Res. Lett., 38, L22802, 2011.
314 Park, J., Helmboldt, J., Grejner-Brzezinska, D. A., Frese, R. R. B. von, and Wilson, T.
315 L.: Ionospheric observations of underground nuclear explosions (UNE) using GPS
316 and the Very Large Array, Radio Sci., 48, 463–469, 2013.
317 Pokhotelov, O. A., Pilipenko, V. A., Fedorov, E. N., Stenflo, L., and Shukla, P. K.:
318 Induced electromagnetic turbulence in the ionosphere and the magnetosphere,
319 Physica Scripta, 50, 600-605, 1994.
320 Pokhotelov, O. A., Parrot, M., Pilipenko, V. A., Fedorov, E. N., Surkov V. V., and
321 Gladyshev V. A.: Response of the ionosphere to natural and man-made acoustic
322 sources, Ann. Geophys., 13, N11, 1197- 1210, 1995.
323 Pokhotelov, O. A., Pilipenko, V. A., and Parrot, M.: Strong atmospheric disturbances
324 as a possible origin of inner zone particle diffusion, Ann. Geophys., 17, 526-532,

1999.

Pulinets, S. A., Boyarchuk, K. A., Hegai, V. V., Kim, V. P., and Lomonosov, A. M.: Quasi-electrostatic model of atmosphere-thermosphere-ionosphere coupling, Adv. Space Res., 26(8), 1209-1218, 2000.

Ritter, P., Lühr, H., and Rauberg, J.: Determining field-aligned currents with the Swarm constellation mission, Earth Planets Space, 65, 1285-1294, 2013.

Ruzhin, Y. Y., Larkina, V. I., and Depueva, A. K.: Earthquake precursors in magnetically conjugated ionosphere regions, Adv. Space Res., 21(3), 525-528, 1998.

Sorokin, V. M., Chmyrev, V. M., and Yaschenko, A. K.: Electrodynamic model of the lower atmosphere and the ionosphere coupling, J. Atmos. Sol. Terr. Phys., 63(16), 1681-1691, 2001.

Xu, T., Hu, Y., Wu, J., Wu, Z., Li, C., Xu, Z., and Suo, Y.: Anomalous enhancement of electric field derived from ionosonde data before the great Wenchuan earthquake, Adv. Space Res., 47(6), 1001-1005, 2011.

Yang, Y.-M., Garrison, J. L., and Lee, S. C.: Ionospheric disturbances observed coincident with the 2006 and 2009 North Korean underground nuclear tests, Geophys. Res. Lett., 39, L02103, 2012.

Zhao, B., and Hao, Y.: Ionospheric and geomagnetic disturbances caused by the 2008 Wenchuan earthquake: A revisit, J. Geophys. Res. Space Phys., 120, 5758–5777, 2015.

Zhang, X., Shen, X., Liu, J., Ouyang, X., Qian, J., and Zhao, S.: Analysis of ionospheric

plasma perturbations before Wenchuan earthquake, Nat. Hazards Earth Syst. Sci., 9, 1259-1266, 2009.

Zhang, X., Shen, X., Zhao, S., Yao, L., Ouyang, X., and Qian, J.: The characteristics of quasistatic electric field perturbations observed by DEMETER satellite before large earthquakes, J. Asian Earth Sci., 79(2), 42-52, 2014.

Zhou, C., Liu, Y., Zhao, S., Liu, J., Zhang, X., Huang, J., Shen, X., Ni, B., and Zhao, Z.: An electric field penetration model for seismo-ionospheric research, Adv. Space Res., 60(10), 2217-2232, 2017.

Figure Captions

Figure 1. The positions of UNE and IGS stations. The position of 3 September 2017 North Korea UNE is represented by black hollow start mark. The locations of IGS stations in both hemispheres are represented by red and blue squares, respectively. Lines of constant geomagnetic latitude are represented by black dashed lines.

Figure 2. An example of time series of relative STEC obtained by SUWN using satellite PRN 28 between 03:00-05:00 UT on 3 September 2017. The explosive time is represented by the red line.

Figure 3. The time sequences of derivatives of relative STEC obtained by SUWN station using satellite PRN 28 between 03:00-05:00 UT on 3 September 2017. (a) first-order derivatives, (2) second-order derivatives, (c) third-order derivatives, and (d) wavelet de-noised third-order derivatives. The explosive time is represented by the red line.

Figure 4. The time sequences of 3-order derivatives of carrier phase derived relative STEC by GNSS observations from different IGS stations in East Asia (left and middle column) and Australia (right column) on 3 September 2017. The blue lines indicate the wavelet de-noised 3-order derivative of relative STEC. The black lines indicate the GPS signal's elevation between the GNSS satellite and IGS stations. The explosive time is represented by the red line.

Figure 5. The IPPs tracks of relative STEC derivatives. The red lines indicate the IPPs tracks obtained by IGS stations in the northern hemisphere. The blue lines indicate the magnetic conjugate positions of the IPPs tracks obtained by IGS stations in the southern hemisphere. The positions of the maximum amplitudes of relative STEC derivatives in the northern hemisphere are represented by red triangles. The geomagnetic conjugate positions of the maximum amplitudes of relative STEC derivatives in the southern hemisphere are represented by blue triangles.

Figure 6. Results of Swarm B ionospheric current data analysis for the 2017 UNE: (a), (c), and (e) are the FAC, (b), (d), (f) are the IRC. From top to bottom, they indicate observations of Swarm B on 19 August 2017 (quiet time), 3 September 2017 (UNE

time), and 18 September 2017 (quiet time), respectively. The ionospheric current disturbances in response to UNE are represented by the red rectangles.

Figure 7. Horizontal distance-time data for the UNE-generated ionospheric disturbances. The black line indicates the fitting curve obtained by the least square method. The gray lines represent the boundaries of 95% confidence intervals. The red and blue triangles indicate same meanings as in Figure 5. The black triangle represents the position of ionospheric current disturbances in the northern hemisphere. The green triangle represents the geomagnetic conjugate position of ionospheric current disturbances in the southern hemisphere.

Figure 8. A sketch of geomagnetic conjugate effect related to UNE in the region of the nuclear test site nearby and the corresponding geomagnetic conjugate region.

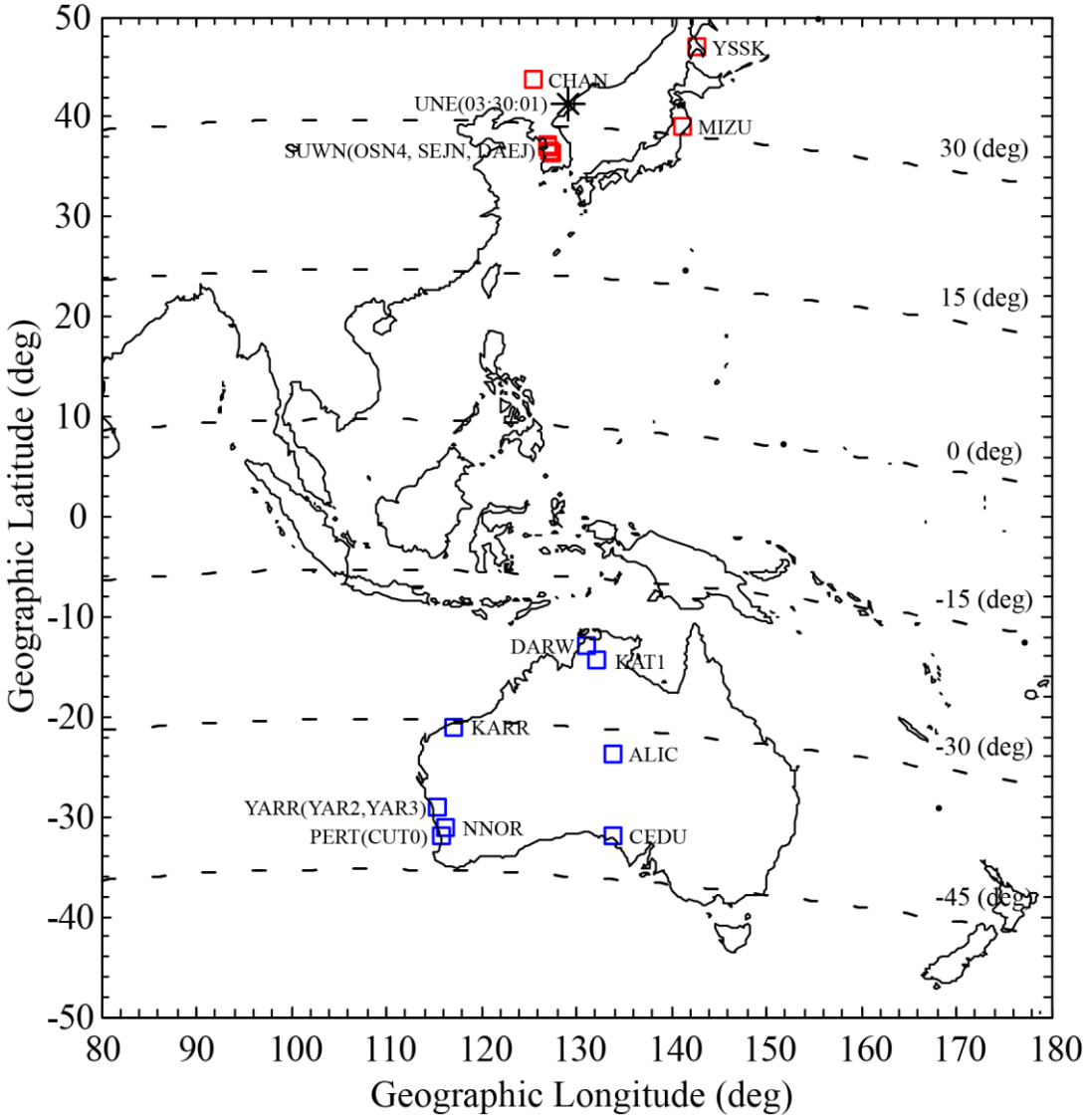

Figure 1. The positions of UNE and IGS stations. The position of 3 September 2017 North Korea UNE is represented by black hollow start mark. The locations of IGS stations in both hemisphere are represented by red and blue squares, respectively. Lines of constant geomagnetic latitude are represented by black dashed lines.

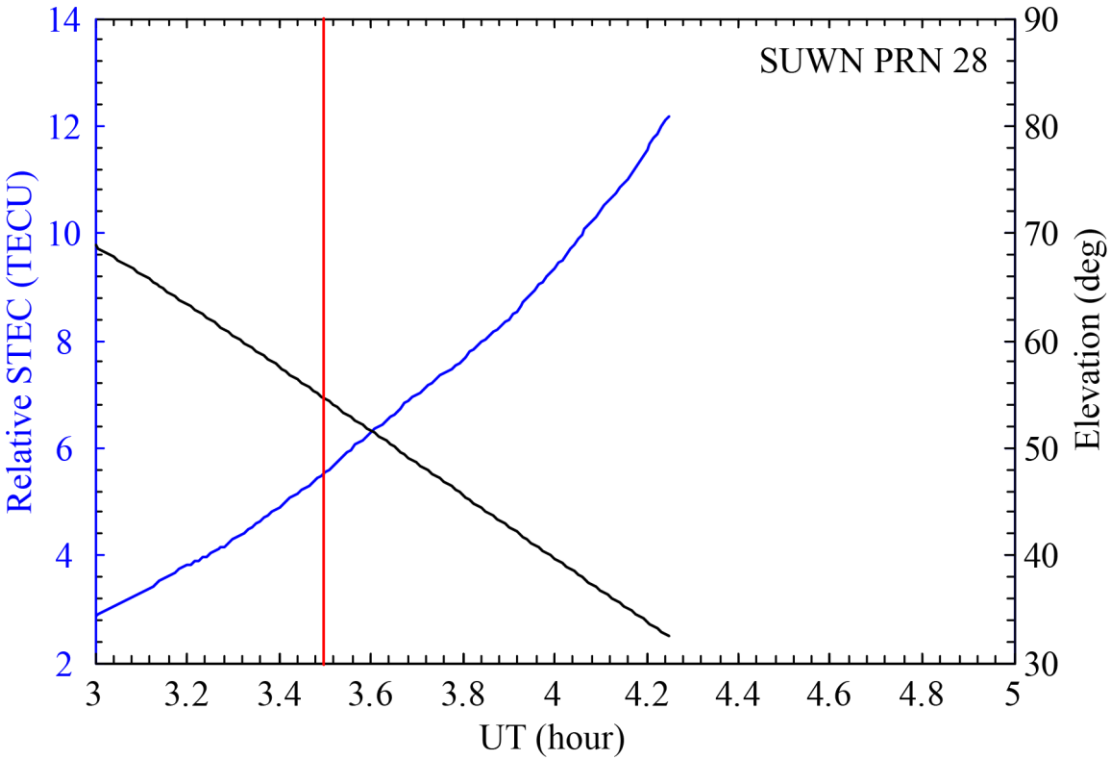

Figure 2. An example of time series of relative STEC obtained by SUWN using satellite PRN 28 between 03:00-05:00 UT on 3 September 2017. The explosive time is represented by the red line.

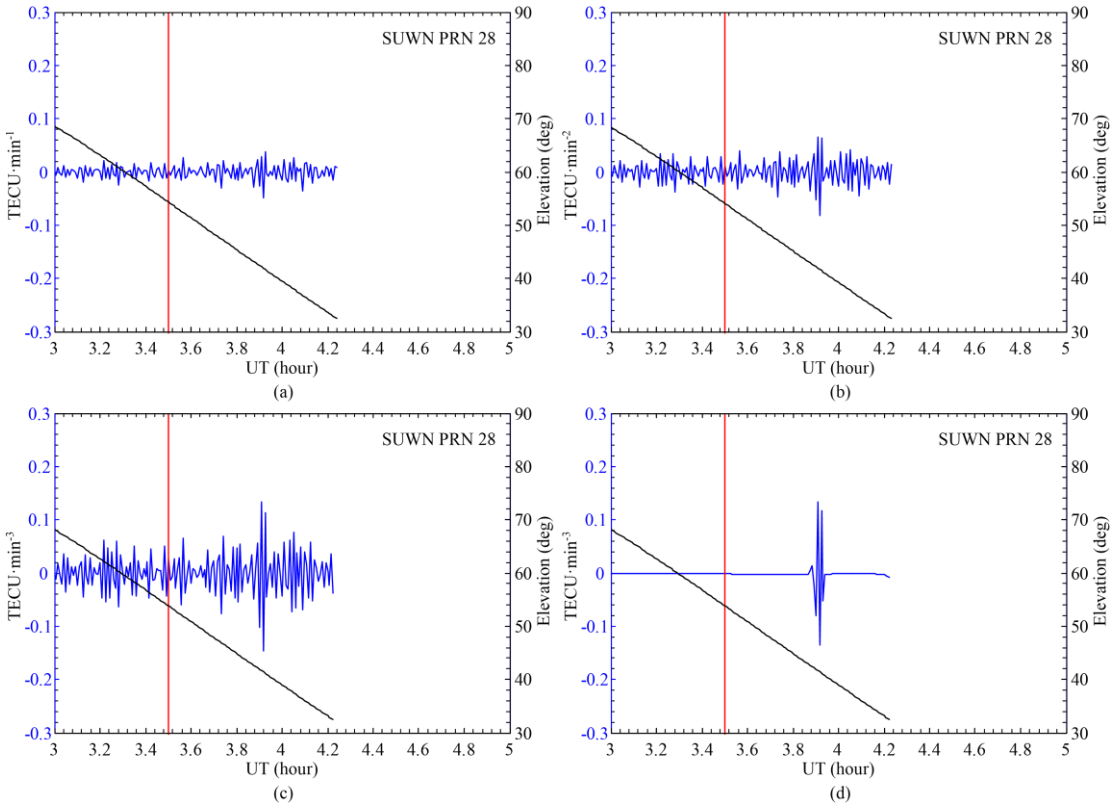

Figure 3. The time sequences of derivatives of relative STEC obtained by SUWN station using satellite PRN 28 between 03:00-05:00 UT on 3 September 2017. (a) first-order derivatives, (2) second-order derivatives, (c) third-order derivatives, and (d) wavelet de-noised third-order derivatives. The explosive time is represented by the red line.

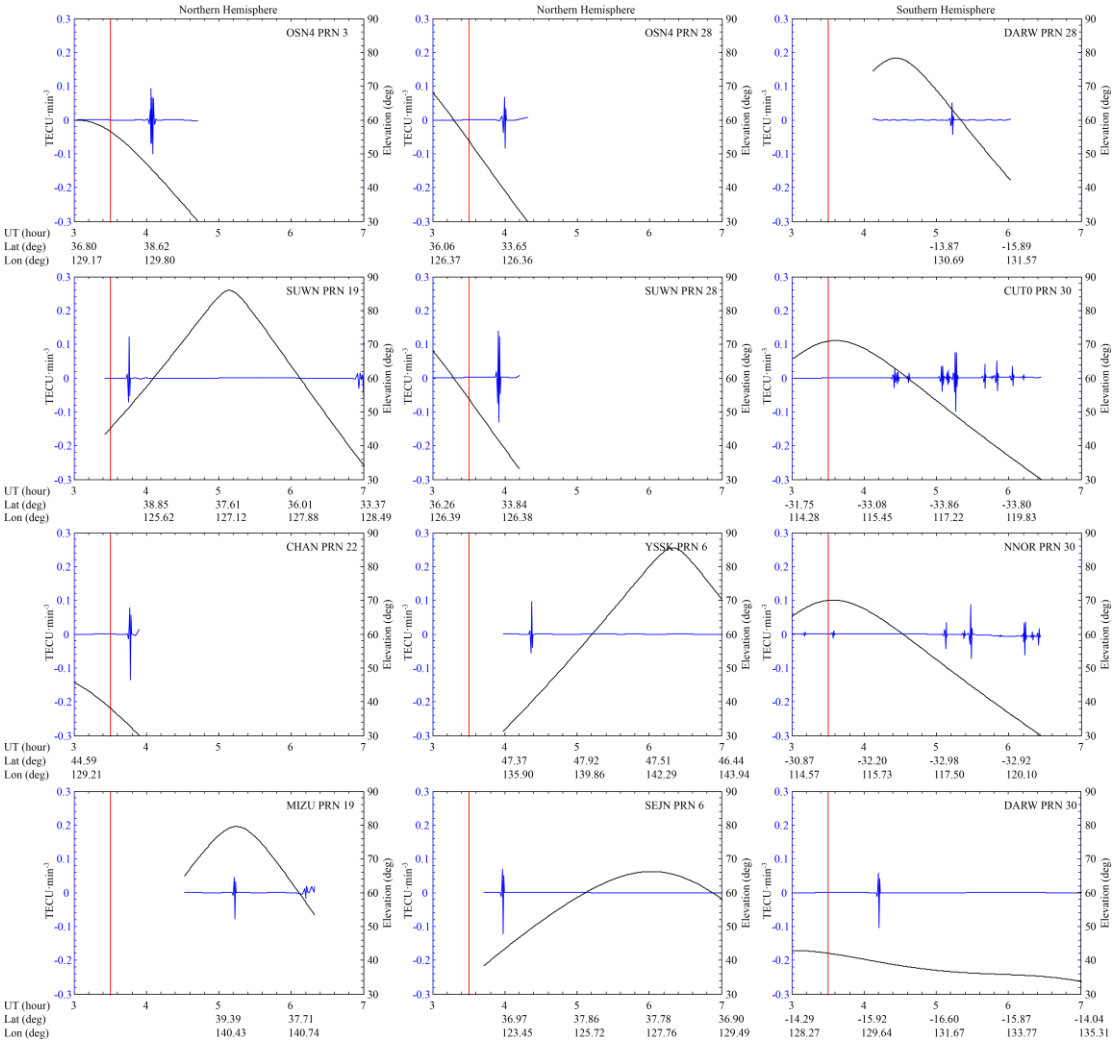

Figure 4. The time sequences of 3-order derivatives of carrier phase derived relative STEC by GNSS observations from different IGS stations in East Asia (left and middle column) and Australia (right column) on 3 September 2017. The blue lines indicate the wavelet de-noised 3-order derivative of relative STEC. The black lines indicate the GPS signal's elevation angle between the GNSS satellite and IGS stations. The explosive time is represented by the red line.

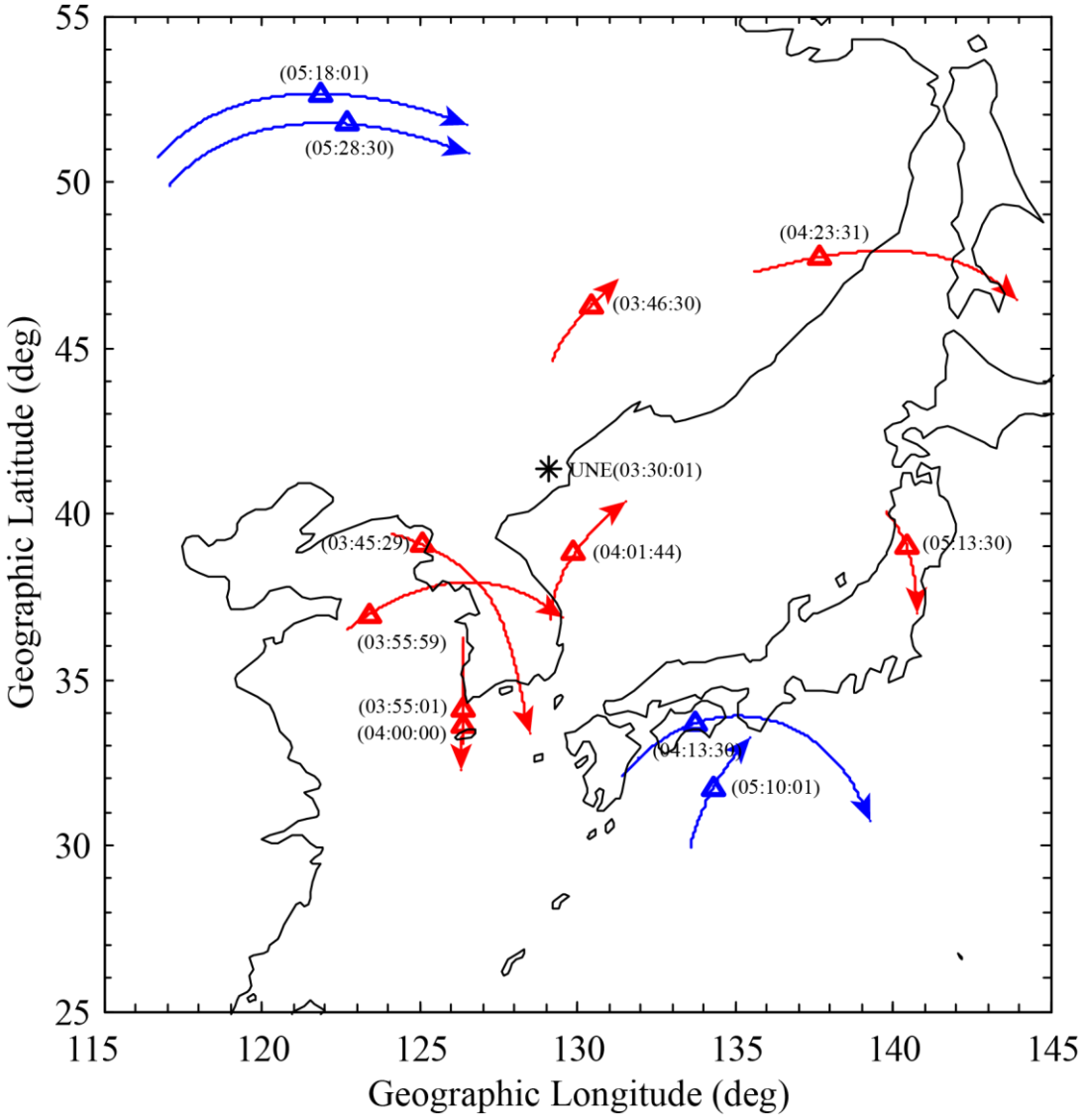

Figure 5. The IPPs tracks of relative STEC derivatives. The red lines indicate the IPPs tracks obtained by IGS stations in the northern hemisphere. The blue lines indicate the magnetic conjugate positions of the IPPs tracks obtained by IGS stations in the southern hemisphere. The positions of the maximum amplitudes of relative STEC derivatives in the northern hemisphere are represented by red triangles. The geomagnetic conjugate positions of the maximum amplitudes of relative STEC derivatives in the southern hemisphere are represented by blue triangles.

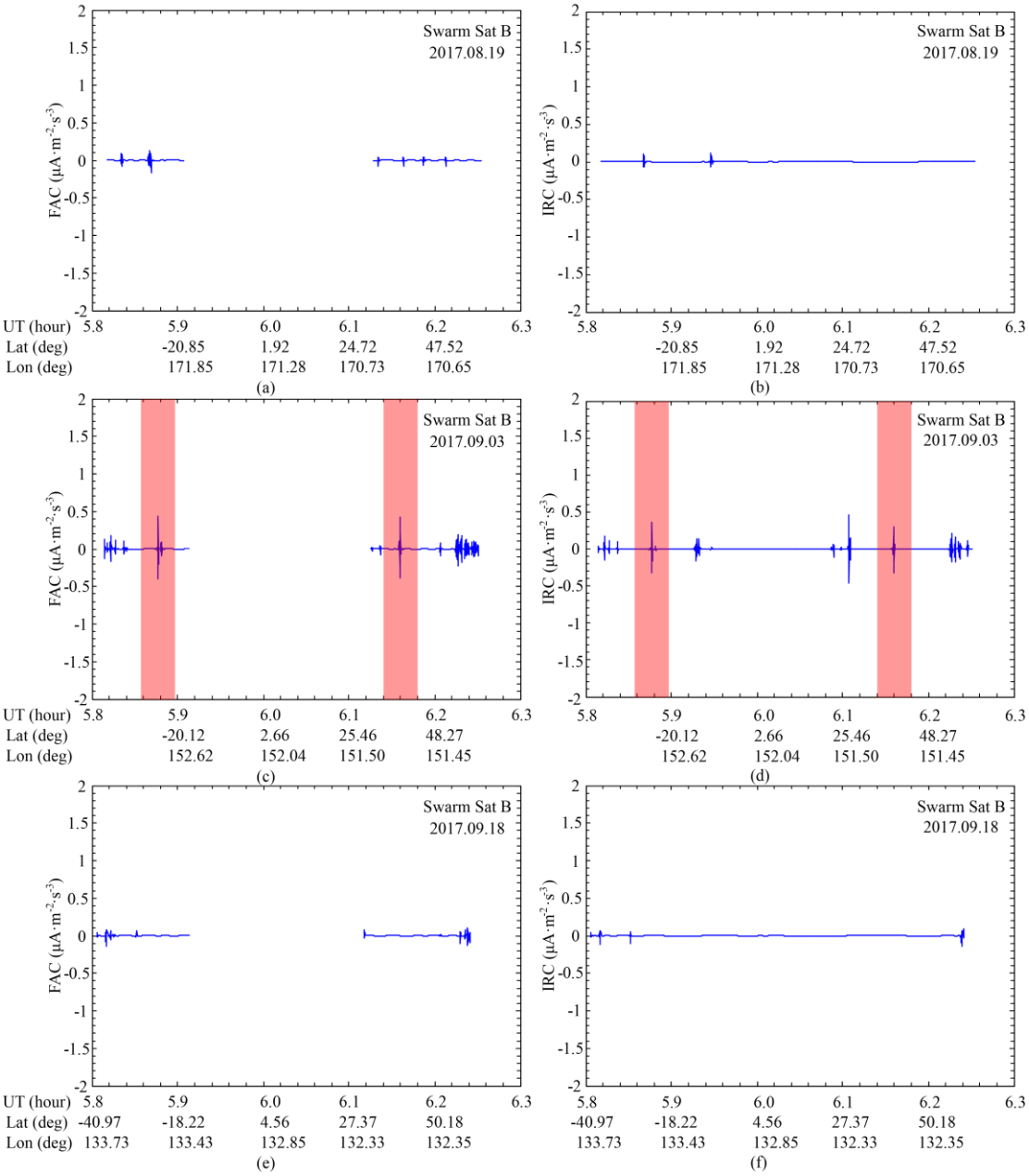

Figure 6. Results of Swarm B ionospheric current data analysis for the 2017 UNE: (a), (c), and (e) are the FAC, (b), (d), (f) are the IRC. From top to bottom, they indicate observations of Swarm B on 19 August 2017 (quiet time), 3 September 2017 (UNE time), and 18 September 2017 (quiet time), respectively. The ionospheric current disturbances in response to UNE are represented by the red rectangles.

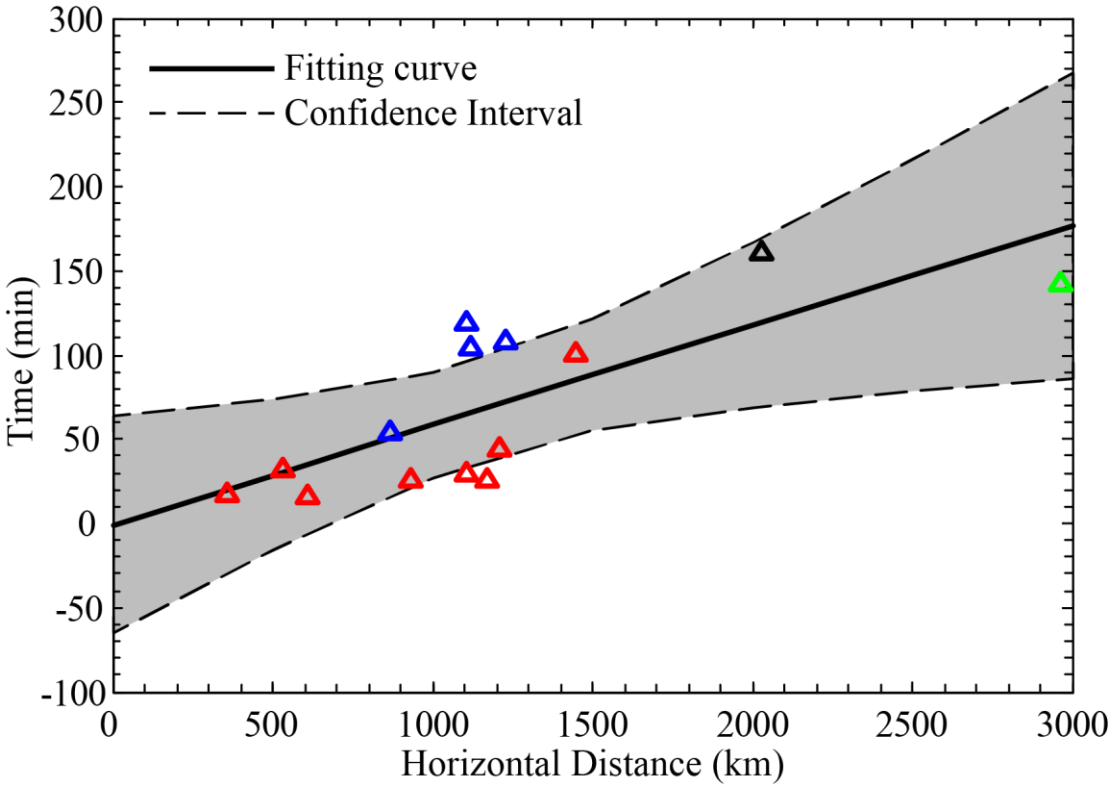

Figure 7. Horizontal distance-time data for the UNE-generated ionospheric disturbances. The black line indicates the fitting curve obtained by the least square method. The gray lines represent the boundaries of 95% confidence intervals. The red and blue triangles indicate same meanings as in Figure 5. The black triangle represents the position of ionospheric current disturbances in the northern hemisphere. The green triangle represents the geomagnetic conjugate position of ionospheric current disturbances in the southern hemisphere.

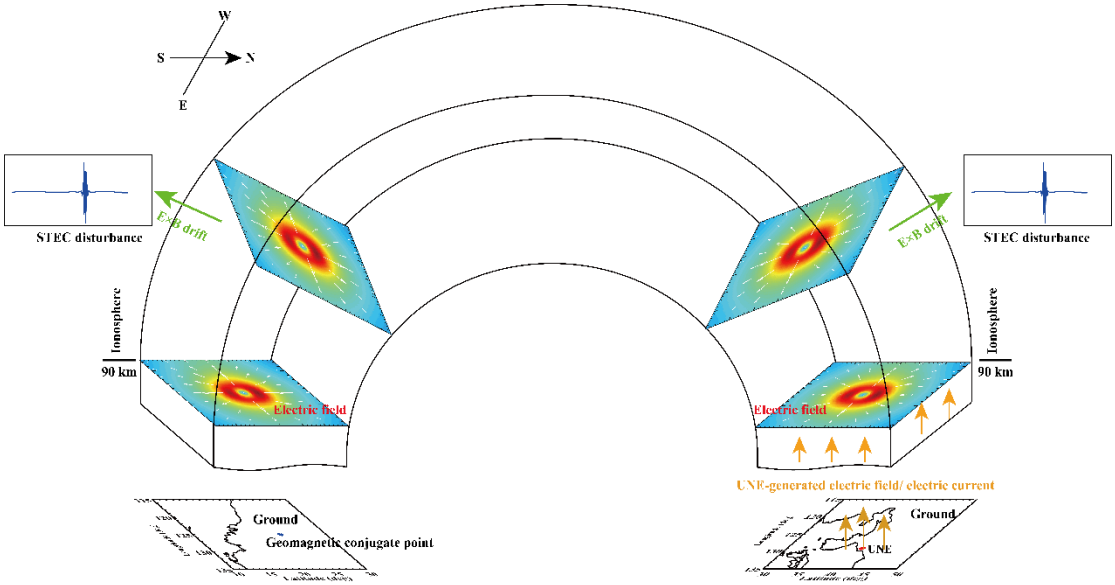

Figure 8. A sketch of geomagnetic conjugate effect related to UNE in the region of the nuclear test site nearby and the corresponding geomagnetic conjugate region.